Quantum Electronics **46** (10) 953–960 (2016)

X-RAY OPTICS DOI: 10.1070/QEL16106

Soft X-ray flat-field VLS spectrographs

E.A. Vishnyakov, A.O. Kolesnikov, E.N. Ragozin, A.N. Shatokhin

Abstract. **We have analysed the capabilities of flat-field spectrometers with concave VLS reflection gratings from the standpoint of spectral imaging in the soft X-ray range. Two types of such instruments are shown to exist: spectrographs with as flat as possible a portion of the focal surface (of Harada spectrograph type) and those with a nearly constant distance from the grating centre to the focal surface, which permits reaching a high spatial resolution with the use of a crossed focusing mirror (without a loss in spectral resolution). Three 0.25, 0.5, and 1.5-m long spectrographs of Harada type were calculated for operation in the ranges 90–250, 50–200, and 20–110 Å, respectively. We show that each of the calculated instruments may be converted to an instrument of the second type for operation in the second and fourth diffraction orders without significant changes in scheme geometry. In this case, the theoretical spatial resolution is equal to ~10 μm throughout the optimisation range.**

Keywords: *laser-produced plasma, soft X-ray radiation, spectral images, concave VLS gratings, flat-field spectrographs, spectral focal surface.*

1. Introduction

Investigations of laser plasmas (including relativistic ones), plasmas of fast electric discharges, active media of soft X-ray (SXR) lasers, cluster plasmas, so-called warm dense matter (WDM) produced by pulses of a free-electron laser, and some other, call for the acquisition of spatially resolved spectral information in the soft X-ray range. Spectra with one-dimensional spatial resolution and spectral images are obtained with an imaging (stigmatic) spectrometer. Previously this task was solved, as a rule, using a grazing-incidence Rowland spectrograph, which was supplemented with a slit aligned perpendicular relative to the direction of the grooves of the diffraction grating. The spatial resolution achievable in this way is limited by radiation diffraction and amounts to ~100 μm for radiation in the 100–200 Å wavelength range; this is achieved at a sacrifice in the recorded radiation flux and brightness of spectral lines.

Meanwhile several experiments call for a spatial resolution of ~10 or even ~1 μm. Examples are provided, for instance, by high-order harmonic generation in relativistic laser plasma irradiated by multiterawatt femtosecond laser pulses [1] and the generation of soft X-ray radiation in the reflection of Ti : sapphire laser radiation from the relativistic plasma wave generated in a pulsed helium jet (relativistic 'flying mirror') [2]. An improvement in spatial resolution is achievable, first, in a spectrometer with a focusing multilayer mirror (MM) and a plane varied line-space (VLS) grating [3] as well as in a spectrometer with a concave VLS grating supplemented with a focusing optical element crossed relative to the grating. An implementation of the instrument of the former type was recently reported at the 15th International Conference on X-Ray Lasers (ICXRL2016) [4], and the latter instrument is the concern of this work.

A flat-field spectrograph is a spectral instrument in which the focal surface is accurately approximated with a plane oriented almost normally (at an angle no more than 20°) to the diffracted radiation. This permits reaching a high resolution with the use of CCD matrices and streak cameras as detectors: the geometrical defocusing vanishes when the sensitive detector surface coincides with the focal plane of the instrument and the near-normal ray incidence on the detector decreases the radiation loss due to absorption in the dead layer of the detector. These drawbacks are inherent in the classical Rowland scheme [5, 6]: for a grazing radiation incidence on a concave diffraction grating, the spectrum is focused on a flat detector also at a grazing incidence (which significantly increases the loss due to absorption in the dead layer) or with a significant geometrical defocusing.

In this work we discuss flat-field spectrographs based on concave reflection gratings with a varied groove spacing which operate in grazing-incidence schemes.

In 1980, T. Harada calculated for the first time a grazing incidence spectrograph with a flat portion of the focal surface corresponding to a wavelength range of 50–200 Å, in which the diffracted rays made relatively small angles with the detector normal [7]. More recently he demonstrated the operation of this spectrograph by recording the spectra of laser plasmas [8]. The spectrograph made use of a spherical VLS grating with a spacing which varied monotonically from 0.99 to 0.69 μm across the 50 mm ruled aperture. The central spatial groove frequency p was equal to 1200 mm^{-1} and the grazing incidence angle – to 3°. This spectrograph became commer-

E.A. Vishnyakov P.N. Lebedev Physics Institute, Russian Academy of Sciences, Leninsky prosp. 53, 119991 Moscow, Russia; e-mail: juk301@mail.ru;
A.O. Kolesnikov, E.N. Ragozin, A.N. Shatokhin P.N. Lebedev Physics Institute, Russian Academy of Sciences, Leninsky prosp. 53, 119991 Moscow, Russia; Moscow Institute of Physics and Technology (State University), Institutskii per. 9, 141701 Dolgoprudnyi, Moscow region, Russia; e-mail: enragozin@gmail.com, shatokhin@gmail.com

Received 29 March 2016; revision received 4 July 2016
Kvantovaya Elektronika **46** (10) 953–960 (2016)
Translated by E.N. Ragozin

cially available and has come to be known as a Harada spectrograph. Later on T. Harada improved his ruling engine and was capable of making gratings with $p \sim 10^4$ mm^{-1} [9], which enabled producing a high-resolution imaging spectrometer for the 250–290 Å range for the Japan space vehicle Solar-B/Hinode [10].

We note that, prior to T. Harada's work on VLS grating fabrication [11], F.M. Gerasimov et al. [12] reported the fabrication of gratings (R = 1 m, p = 300 and 600 mm^{-1}) with a total relative spacing variation at a level of $\sim 10^{-2}$. This relatively small spacing variation permits compensating for astigmatism in normal-incidence schemes.

Recently, a high-resolution flat-field spectrograph was made for recording the spectra of laser-produced plasmas in the 10–50 Å range at the Lawrence Livermore National Laboratory (USA) [13]. A cooled CCD matrix was employed as a detector. Radiation was dispersed with a concave spherical (radius of curvature R = 44.3 m) VLS grating with an average spatial groove frequency of 2400 mm^{-1} mounted at a grazing angle of $\sim 2°$. The complete parameter set of the optical scheme of Ref. [13] was not reported.

Among the papers that reported achievements reached with the use of VLS gratings, mention should be made of the works of M. Hettrick et al. [14, 15]. They described a stigmatic spectrograph for the observation of extrasolar objects in the 70–760 Å range and several astigmatic laboratory spectrometers of ultrahigh ($\sim$35000) resolving power. Recently M. Hettrick came up with the idea of a monochromator with a plane VLS grating containing no other optical elements [16].

The aim of our work is to analyse the capabilities of concave spherical VLS gratings for spectral diagnostic research in the VUV and SXR ranges and to design a set of spectrographs with different parameters, bearing in mind the making of the instruments of this class in the future.

2. Control of focal surface curvature: analytical approach

Let the spatial groove frequency of a VLS grating be described by a polynomial dependence on the y coordinate (Fig. 1):

$$p(y) = p_0 + p_1 y + p_2 y^2 + p_3 y^3 + \dots , \tag{1}$$

with $dn/dy = p(y)$, where n is the groove number. Assuming that the source is in the principal diffraction plane, we consider the beam which lies entirely in the principal plane. Let a point source be at point A and point B be its spectral image at a wavelength λ (Fig. 1). Point P belongs to some arbitrary grating groove; the grooves are assumed to be infinitely thin lines, as is commonly done in the derivation of the focusing grating properties and the aberrations of the wave front. The optical path function

$$F = l_1 + l_2 + m\lambda n(y), \tag{2}$$

where l_1 and l_2 are the distances AP and PB, respectively, and m is the order of diffraction. For the sum $l_1 + l_2$ we take advantage of the expansion borrowed from Ref. [17]:

$$l_1^2 = r^2 + x^2 + y^2 - 2xr\sin\varphi + 2yr\cos\varphi, \tag{3}$$

$$l_2^2 = r_h'^2 + x^2 + y^2 - 2xr_h'\sin\psi - 2yr_h'\cos\psi, \tag{4}$$

where r is the source–grating distance (AO in Fig. 1); r_h' is the distance to the spectral (horizontal) focus (OB); φ and ψ are grazing angles of incidence and diffraction of the central ray. Since the VLS grating is spherical (with the radius of curvature R), the coordinates of point P(x, y) are bound by the equation

$$(x - R)^2 + y^2 = R^2, \tag{5}$$

which permits expressing the x coordinate in terms of y. Then, expanding expression (2) in a Taylor series in y up to terms y^4 and applying the Fermat principle ($\partial F/\partial y = 0$) gives the following expressions:

$$\cos\varphi - \cos\psi = m\lambda p_0, \tag{6}$$

$$\frac{\sin^2\varphi}{r} - \frac{\sin\varphi}{R} + \frac{\sin^2\psi}{r_h'} - \frac{\sin\psi}{R} = m\lambda p_1, \tag{7}$$

$$\frac{3}{2}\left[\frac{\cos\varphi}{r}\left(\frac{\sin^2\varphi}{r} - \frac{\sin\varphi}{R}\right) - \frac{\cos\psi}{r'}\left(\frac{\sin^2\psi}{r'} - \frac{\sin\psi}{R}\right)\right]$$

$$+ \frac{1}{2R^2}\left(\frac{1}{r} - \frac{\sin\varphi}{R} + \frac{1}{r'} - \frac{\sin\psi}{R}\right) = -m\lambda p_2, \tag{8}$$

$$2\left[\left(\frac{\cos\varphi}{r}\right)^2\left(\frac{\sin^2\varphi}{r} - \frac{\sin\varphi}{R}\right) + \left(\frac{\cos\psi}{r'}\right)^2\left(\frac{\sin^2\psi}{r'} - \frac{\sin\psi}{R}\right)\right]$$

$$- \frac{1}{2r}\left(\frac{\sin^2\varphi}{r} - \frac{\sin\varphi}{R}\right)^2 - \frac{1}{2r'}\left(\frac{\sin^2\psi}{r'} - \frac{\sin\psi}{R}\right)^2 = m\lambda p_3. \tag{9}$$

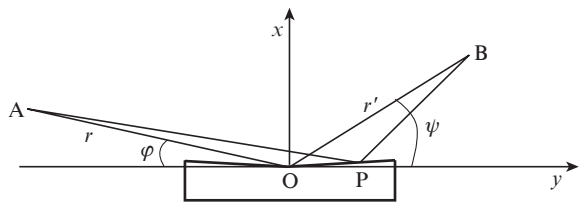

Figure 1. Construction of a spectral image by a concave VLS grating; O is the centre of the spherical VLS grating and the origin of xy coordinate system. A point source is at point A, point B is its spectral image. Point P(x, y) belongs to an arbitrary grating groove, and φ and ψ are the grazing angles of incidence and diffraction of the central ray.

The system of equations (6), (7) is well known; it defines the shape of the spectral focal curve. Equation (6) (the grating equation) describes the direction of diffraction of the central ray and Eqn (7) – the location of the paraxial spectral (horizontal) focus r_h'. Expressions (8), (9) were obtained for the terms of expansion of the optical path function F (2) in powers y^3 and y^4 with allowance for Ref. [17]. They describe the conditions whereby the meridional coma (8) and the spherical aberration (9) of a monochromatic beam lying in the principal plane are equal to zero.

We note an important feature of the form of notation of Eqns (6)–(9). The left-hand sides of all equalities contain only the geometrical characteristics of the instrument (the radius R

of curvature of the grating, the distances to the source and the image, angles φ and ψ), while the right-hand sides contain only the terms of the form $m\lambda p_i$. This signifies the following: once an attempt to design a felicitous instrument geometry meets with success, it may immediately be transferred to any other wavelength λ_0 by simple proportional scaling of all terms of expansion of $p(y)$ (1). However, this would require the fabrication of a new grating.

It turns out that the shape of the instrument's spectral focal surface depends only on the p_1/p_0 coefficient ratio, the grazing incidence angle φ, the radius R of curvature of the grating, and the distance r of the entrance slit from the grating centre. It is easily verified that the aberrations are compensated for certain values of the ratios p_2/p_0 and p_3/p_0 for a fixed diffraction angle ψ. Consequently, a proportional increase or decrease in all grating coefficients would not change the spectral line image for the same diffraction angle but would change its corresponding wavelength.

3. Numerical calculation technique

To design and optimise spectrographs with a concave spherical VLS grating (spectrographs of Harada type) with a flat field in the working spectral range we adhered to the following procedure. At the first stage we define the working spectral range $\Delta\lambda$ as well as the angle φ and the radius R of curvature, which determine the spectral resolution and the outer dimensions of the instrument. Next, by varying coefficients p_1, p_0 and using Eqns (6), (7) we calculate the modified spectral focal curve, which deviates from the Rowland circle (Fig. 2). A portion of the focal curve flattens out and becomes practically perpendicular to the y axis (the portion of the $p_1 = 16.55$ curve in the interval 90–250 Å in Fig. 2); in this case, the incident rays make angles with the normal within $\pm 20°$.

After defining the location of the spectral focal curve, we calculated the optimal position of the detector plane (by the least root-mean-square method or by minimising the maximal geometrical defocusing in the spectrum). Then, coefficients p_2 and p_3 were calculated from formulas (8), (9) to zero the aberration of meridional coma and the spherical aberration at some optimisation wavelength λ_{opt} selected from the middle of the range $\Delta\lambda$.

Here, the analytical stage of calculation ends up and is followed by an analysis of the spectral images of the entrance slit obtained by numerical ray tracing. Use was made of the SHADOWVUI extension of X-Ray Oriented Programs (XOP) Software Package v.2.3 (available for free download on the ESRF website [18]).

First of all, numerical ray tracing was performed at a wavelength λ_{opt}; after that, the coefficient p_3 was defined more precisely and the coefficient p_4 was fitted to minimise the dimension (the base width) of the simulated spectral image. Then we selected 'reference' wavelengths λ_f (the wavelength of focusing), λ_d (the wavelength of maximum defocusing), and λ_{min}, λ_{max} (the boundaries of the spectral range $\Delta\lambda$), at which spectral images were obtained by numerical ray tracing. In a number of cases some of these wavelengths coincided.

In practice the calculation and optimisation were inherently iterative due to the possibility of additional manipulation of some parameters. For instance, the distance of the entrance slit from the VLS grating may differ from the Rowland case $R\sin\varphi$. The wavelength λ_{opt}, which is free from meridional coma and spherical aberration, may also be varied.

4. Results and their discussion

Figure 2 serves to illustrate the behaviour of the spectral focal curve in relation to the VLS grating parameter p_1. In this case, the VLS grating is mounted at a grazing angle of 4° at a distance of 130 mm from the source. The average spatial groove frequency p_0 =1200 mm^{-1} and the radius of curvature of the grating $R = 2$ m. The origin is at the grating centre. The lower line corresponds to the Rowland circle of a classical concave grating with $R = 2$ m. The rays emanating from the grating centre indicate the directions of diffraction for different $m\lambda$ values.

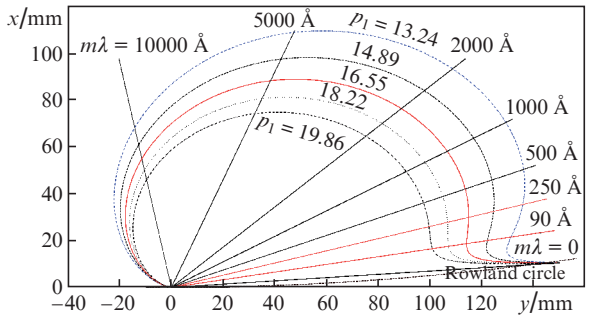

Figure 2. Behaviour of the spectral focal curves in the compact version of a flat-field grazing-incidence spectrograph (version 1) under variation of the parameter p_1. The portion of the middle curve between the 90 and 250 Å rays is well approximated with a straight-line segment.

Referring to Fig. 2, with increasing $m\lambda$ all focal curves promptly deviate from the Rowland circle and become flat in the 90–250 Å curve piece oriented at some angle to the incident rays. For $p_1 = 16.55$, this piece of the focal curve is nearly perpendicular to the incident rays (departure from the normal ~15°), which permits employing a CCD matrix as the detector in this scheme. The class of spectrographs that make use of this flat portion of the focal curve will be referred to as Harada spectrographs (Fig. 3a). The value $p_1 = 16.55$ was selected as the optimal one, because it maximises the length of the flat-field spectral region.

Interestingly, by fitting p_1 it is possible to orient the focal curve normally to the incident rays in some wavelength range. In this case, the focal surface is approximately spherical; by increasing distance L_2 (Fig. 3b) it is possible to diminish the difference between the focal surface and the approximating plane, so that the dimension of the spectral image of the source is of the order of the pixel size (13 μm) of a CCD matrix for all wavelengths within the $\Delta\lambda$ range. This class of spectrographs permits obtaining a high spatial resolution with the use of an additional focusing mirror (element M in Fig. 3b) crossed relative to the VLS grating.

We emphasise that the behaviour of spectral focal curves and their dependence on p_1 (see Fig. 2) are universal and are common for all VLS spectrographs calculated in our work. Figure 4 depicts the characteristic departures of the focal surface from the optimal detector plane and the positions of the

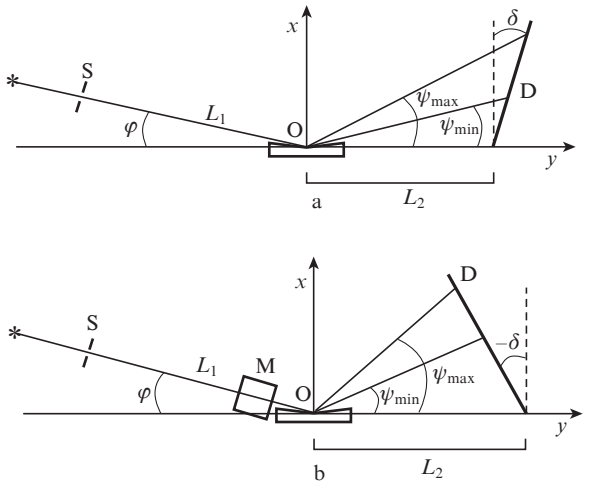

Figure 3. Arrangement of optical elements in an astigmatic Harada spectrograph (a) and in a quasi-stigmatic spectrograph with normal incidence of rays on a detector (b) (S is the entrance slit, D is the detector, L_1 is the length of segment SO, M is the crossed focusing mirror).

'reference' lines for the two instrument classes under discussion. One can see that the number of 'reference' lines may vary: usually there are five of them (λ_{f_1}, λ_{d_1}, λ_{opt}, λ_{d_2}, λ_{f_2}) in Harada spectrographs and three (λ_{f_1}, λ_{opt}, λ_{f_2}) in the instruments with spatial resolution. Figure 4b shows the spectral and spatial focal curves; the latter was obtained with the inclusion of a crossed mirror.

We calculated a family of spectrographs for the ranges 90–250, 50–200, and 20–110 Å (the overall lengths of the instruments are equal to 0.25, 0.5, and 1.5 m, respectively).

4.1. Flat-field VLS spectrographs

Flat-field Harada spectrographs were calculated proceeding from different requirements (Table 1, versions 1–3). Version 1 is a compact device of short length; in Version 2 the length of the working spectral range is matched to the size of the sensitive area of our CCD detector (27 mm); Version 3 is a short-wavelength long-focus instrument ($\Delta\lambda$ = 20–110 Å).

All geometrical characteristics of the instruments (L_1, L_2, φ, δ, etc.), their working ranges $\Delta\lambda$, VLS-grating parameters, as well as resolving powers and plate scales are collected in Table 1. The boundary wavelengths λ_{min} and λ_{max} of the working spectral range are also reference lines of the spectrographs, like λ_f and λ_d, but they are not represented separately in Table 1. The problem of an optimal VLS-grating width w_{opt} (w_{theor}) is discussed below.

By way of example Fig. 5 depicts the spectral images of a point monochromatic source at the 'reference' wavelengths λ_{min} = 90 Å, λ_{opt} = 143 Å , and λ_{d_2} = 180 Å for the Version-1 spectrograph (a compact 0.25-m long device). One can see that all the images of the point monochromatic source are confined in the typical CCD detector pixel size (13 μm). The defocusing is greatest at a wavelength λ_{max} = 250 Å. In this case, the size of the spectral image amounts to 19 μm (fits into two CCD detector pixels). The average spectral resolution $\delta\lambda$ = 0.18 Å.

In the Version-2 spectrograph the working spectral range $\Delta\lambda$ = 50–200 Å was selected from considerations of convenience of performing experiments, when the entire spectrum fits into the sensitive detector area. However, the spectral focal surface also remains flat in a broader wavelength range (50–275 Å). The maximal geometrical defocusing in the spectrum does not exceed 16 μm and is at λ_{max} = 275 Å, which permits operation also in the 200–275 Å range without a loss in spectral resolution. In this case, however, the total width of the spectrum (38 mm for $\Delta\lambda$ = 50–275 Å) will exceed the CCD detector area (27 mm).

The Version-3 spectrograph was designed as a short-wavelength long-focus instrument. It yields a theoretical resolving power of $\sim 5 \times 10^3$ and spans more than two octaves in wavelength ($\Delta\lambda$ = 20–110 Å). The spectral images of a point monochromatic source at all 'reference' lines, with the exception of λ_{min} and λ_{max}, fit into a CCD detector pixel size of 13 μm. For λ_{min} and λ_{max} the images fit into two pixels (see Table 2). We note that the Version-3 spectrograph is the most 'off-Rowland' spectrograph among the Harada instruments designed in this work.

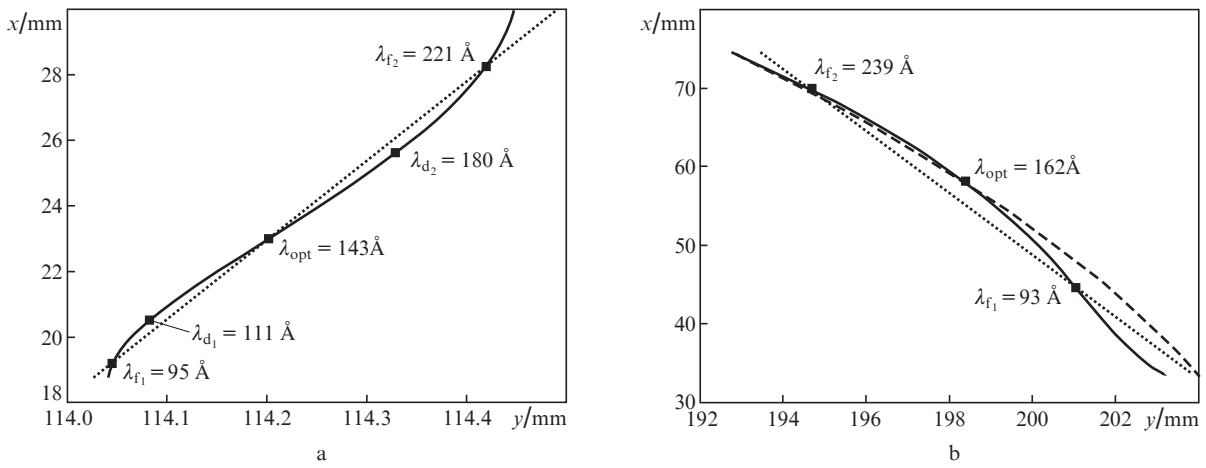

Figure 4. Typical behaviour of the focal surfaces near the detector plane. Version of a flat-field spectrograph (of Harada type) (a) and spectrograph version with a nearly constant VLS grating–detector distance (b). The dotted line indicates the detector plane, the solid curve stands for the spectral focus and the dashed line – for the spatial focus.

Table 1. Design parameters of flat-field VLS spectrographs.

Parameters		Harada spectrographs			Spectrographs with spatial focusing		
		Version					
		1	2	3	1a	2a	3a
Length/mm		250	502	1500	234	456	1391
$\Delta\lambda$/Å		90–250	50–200	20–110	90–250	50–275	20–125
'Reference' wavelengths/Å	λ_{opt}	143	125	48	170	162	73
	λ_f	95; 221	64; 152	25; 99	116; 227	92; 239	33; 105
	λ_d	111; 180	90	33; 73	–	–	–
Angle of incidence φ/deg		4	3	2	4	3	2
L_1/mm		130.0	252.0	750.0	130.0	252.0	750.0
L_2 /mm		112.5	250.0	750.0	104.2	212.3	664.8
δ/deg (see Fig. 3)		4.7	0.0	0.0	–10.4	–14.5	–12.3
$\psi_{min} - \psi_{max}$/deg		9.3–14.6	7.0–12.9	6.0–13.3	12.6–20.4	9.4–21.2	7.0–12.9
Angle of incidence on detector $\psi + \delta$/deg		14.0–19.3	7.0–12.9	6.0–13.3	2.2–9.0	–5.1–6.7	–5.3–0.6
Optimal grating width W_{opt} (W_{theor})/mm		30 (24)	50 (48)	60 (120)	30 (24)	10 (48)	10 (120)
R/m		2	6	30	2	6	30
p_0/mm^{-1}		200	1200	2400	1200	1200	2400
p_1/mm^{-2}		16.548	8.000	5.634	19.857	10.400	6.761
p_2/mm^{-3}		0.2042	0.0440	0.0106	0.2751	0.0710	0.0149
$p_3/10^{-4}$ mm^{-4}		25.00	2.28	0.19	36.20	5.00	0.29
$p_4/10^{-6}$ mm^{-5}		22.70	1.50	0.035	37.04	3.70	0.05
Average plate scale/Å mm^{-1}		14.14	5.58	0.90	10.00	5.32	0.78
Dimensions of grating aperture, width × height/mm		30 × 10	50 ×18	60 × 18	30 ×10	10 ×18	10 ×18
Resolution $\delta\lambda$/Å		0.18	0.07	0.01	0.26	0.14	0.02
Resolving power $\lambda_{opt}/\delta\lambda$		794	1785	4800	654	1157	3650

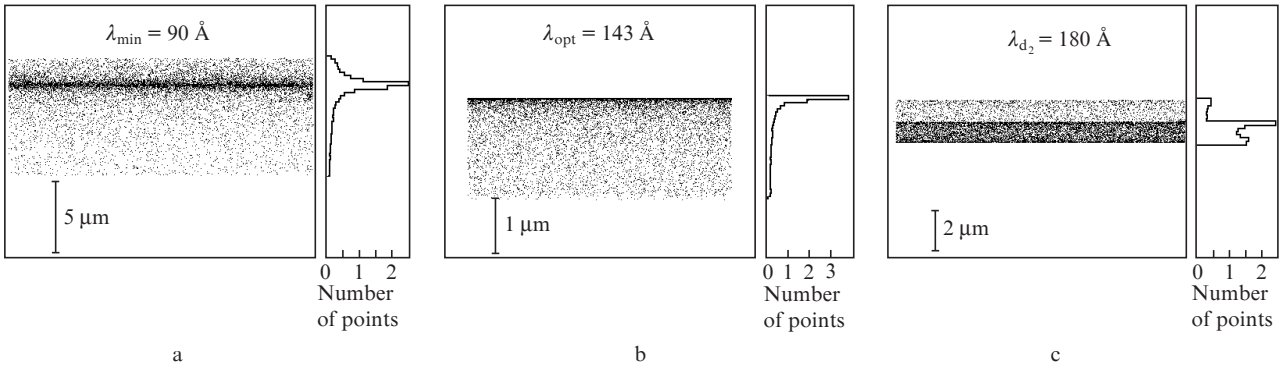

Figure 5. Spectral images at wavelengths λ_{min}, λ_{opt}, and λ_{d_2} produced by a point source located in the plane of the entrance slit (Version 1 of the compact Harada spectrograph); one scale division corresponds to 500 points in Figs 5a and 5c and to 1000 points in Fig. 5b.

When the entrance slit in the Version-3 spectrograph is placed on the Rowland circle (Version 3r), its distance from the VLS grating increases approximately twofold, while the detector distance from the grating is hardly changed. Simultaneously the angular dimension of the flat-field region becomes narrower, which shortens the working spectral range by 20 Å (to $\Delta\lambda = 20-90$ Å). In this case, the optimal value of coefficient p_4 tends to zero, which may simplify the fabrication of VLS gratings by interference lithography techniques.

Table 2 gives the dimensions of the spectral images of a point monochromatic source at 'reference' wavelengths for all VLS spectrograph versions, including Version 3r considered above. The size of resultant image is defined by geometrical defocusing as well as by aberrations at a given wavelength. In Harada spectrograph Versions 1 and 2, the

Table 2. Theoretical (ray-trace) widths (μm) of the spectral images for different VLS spectrographs. The image size in the crossed (spatial) direction is enclosed in parentheses.

'Reference' wavelengths*	Harada spectrographs				Spectrographs with spatial focusing		
	Version						
	1	2	3	3r	1a	2a	3a
λ_{min}	8	45	19	10	20 (9)	49 (10)	20 (16)
λ_{f_1}	6	18	4	3	10 (6)	33 (8)	11 (16)
λ_{d_1}	3	7	6	5	–	–	–
λ_{opt}	2	4	0.5	1	12 (7)	15 (10)	15 (17)
λ_{d_2}	2	–	13	5	–	–	–
λ_{f_2}	10	10	3	5	28 (16)	20 (18)	5 (19)
λ_{max}	19	15	19	17	47 (20)	32 (22)	21 (20)

*'Reference' wavelengths are given in Table 1.

role of aberrations rises sharply as we recede from λ_{opt} and approach the edges of the $\Delta\lambda$ range, which tends to blur the images focused at λ_{f_1} and λ_{f_2}. In the case of Versions 3 and 3r, aberrations are less significant and the geometrical effect prevails.

4.2. VLS spectrographs with spatial focusing

As discussed above, the working portion of the spectral focal curve of a VLS spectrograph may be chosen in favour of the portion with a near-normal ray incidence on the detector, bearing in mind the attainment of the highest spatial resolution with a crossed concave mirror. Referring to Fig. 2, this case corresponds to the portion of the $p_1 = 19.86$ curve between the rays with $m\lambda = 250$ and 500 Å as well as to the portions between 500 and 1000 Å rays in all curves plotted in the drawing. When we are dealing with the recording of spectra in the 125–250 Å interval, the instruments under discussion are supposed to operate in the second or fourth orders of diffraction.

Presented in the right part of Table 1 are the versions of VLS spectrographs (1a–3a) adapted for the operation with crossed spatial focusing in the second order of diffraction. In Versions 2a and 3a the working spectral ranges turned out to be broader than in cases 2 and 3, because they were designed from considerations of maximising the length of the portion of the spectral focal surface which was nearly normal to the incident rays. In this case we did not impose the requirement that the length of the spectrum should match the sensitive detector area size.

The use of the portion of the focal surface with normal incidence of the rays diffracted by the VLS grating (Versions a) permits using a high spatial resolution (~10 μm) in the operation with a compact source, which corresponds to the CCD detector pixel size. The spatial focusing for a point source placed 63 mm in front of the entrance slit is exemplified in Figure 6 in Version 1a (the horizontal and vertical scales in Fig. 6 are significantly different). The spatial focusing is effected with a concave mirror ($R = 2$ m, $W = 20$ mm) mounted at a grazing angle of 4.26° and crossed relative to the VLS grating (see Fig. 3b).

The mirror geometry should satisfy a number of requirements. The radius of curvature should be the same as for the VLS grating, while the central mirror–grating distance should exceed the half-sum of their widths (by 20–45 mm)

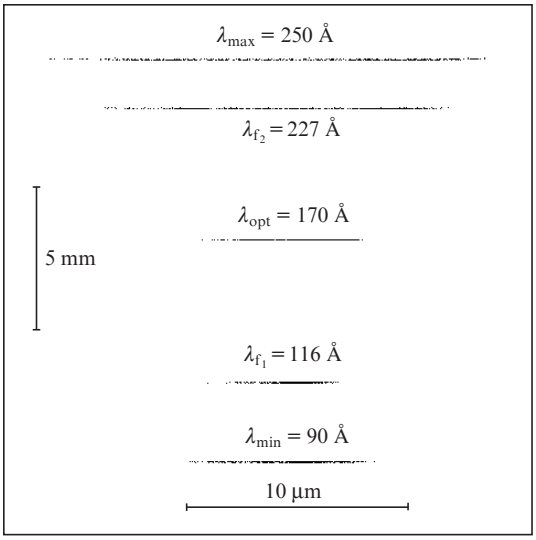

Figure 6. Example of spatial focusing of the image of a point source at 'reference' wavelengths for Version-1a VLS spectrograph.

but should not be too long, so as not to position the source too far from the slit. The source–mirror path length of the central ray is equal to its subsequent path length to the detector; hence we found the source–slit distance (see Fig. 3b). The equal angles of incidence and reflection were found from the condition that the source was located on the Rowland circle of the mirror.

Given in the right part of Table 2 are the image dimensions of a point monochromatic source on the detector in spectral and spatial directions for the designed VLS spectrograph versions with spatial focusing. One can see that the addition of the focusing mirror slightly deteriorates the spectral focusing (to three-four CCD detector pixels), but the spatial resolution is ~10 μm (one-two pixels) in this case.

We note that it is possible to obtain spatial resolution also in a Harada spectrograph with the use of a crossed mirror (Versions 1–3). Since the rays diffracted by the VLS grating make an angle of no more than 20° with the detector normal in Harada schemes, the path length and the grating–detector distance depend slightly on λ. For instance, in Version 2 the difference of the path lengths for $\lambda = 50$ and 200 Å amounts to

only 4.65 mm, which is much shorter than the grating–detector distance (250 mm). That is why the addition of a crossed focusing mirror will increase the spectrum intensity and provide a spatial resolution of ~20 μm. In this case, the field of view will amount to 3–10 mm (depending on the VLS spectrograph version).

In all designed VLS spectrograph versions the working spectral range covers more than an octave in wavelength. If no special measures are taken, this may pose problems in the identification of wavelengths in the resultant spectra due to the overlapping of different orders of diffraction. The use of a MM as the crossed mirror will solve this problem by extracting different spectral ranges in different experiments [19, 20]. For instance, in Version 1 ($\Delta\lambda = 90–250$ Å) use can be made of a Mo/Si MM [21, 22] for the 125–250 Å range as well as of a Sb/B_4C MM [23] for the 90–125 Å range without changing the VLS grating.

4.3. Aberrations and optimal VLS-grating width

Recall that complete compensation of aberrations (8), (9) is possible for only one wavelength (more precisely, for only one angle of diffraction ψ_{opt}), for other λ the aberrations are approximately compensated for. That is why the shape of the spectral image of a point monochromatic source will vary with λ, since the aberrations depend only on the angle of diffraction ψ (for the selected p_1/p_0, p_2/p_0, and p_3/p_0 ratios).

Because of the prompt growth of aberrations with deviation of local diffraction angles ψ from ψ_{opt}, there exists an optimal grating width, whereby the maximal resolving power is realised without a sacrifice in line irradiances. For classical concave diffraction gratings in the Rowland scheme, this width is theoretically calculated by formula [24]

$$W_{theor} = 2.42\left[\lambda R^3 \frac{\sin\varphi \sin\psi}{(1-\sin\varphi\sin\psi)(\sin\varphi+\sin\psi)}\right]^{1/4}. \quad (10)$$

The data given in the line 'Optimal grating width' in Table 1 suggest that formula (10) is of limited application for VLS gratings. This is due to the influence of coefficients p_2, p_3, and p_4 on aberrations at different diffraction angles ψ. While it is possible to cancel aberrations at certain wavelengths, the aberrations at other λ may be unintentionally enhanced, which is improved by limiting the working area of the VLS grating.

The optimal VLS grating width W_{opt} in Version 1 spectrograph exceeds W_{theor} by 25%, in Version 2 W_{theor} and W_{opt} are practically the same, and in Version 3 W_{opt} is two times narrower than W_{theor}. In the case of VLS spectrographs with spatial resolution the limitations on W_{opt} are even more stringent (see Table 1). In Version 1a the image size in the spectral direction is only slightly longer (in comparison with Version 1) and fit into two detector pixels for the same W_{opt}. In Versions 2a and 3a, obtaining a spectral resolution of about two detector pixels requires that W_{opt} should not exceed 10 mm, which is much narrower than the optimal grating width W_{theor} in the classical case.

In the selection of the VLS grating coefficient p_3 it was noticed that the spectral image at a wavelength λ_{opt} for $W_{opt} > 10$ mm in Versions 2a and 3a takes on an unconventional form. Instead of one characteristic intensity distribution peak there appear two–three (like in Fig. 5c), whose separation may exceed the detector pixel size. Narrowing the grating width to 10 mm removes the undesired maxima and permits obtaining a resolution at a level of two detector pixels. In Version 3a, the geometrical defocusing at a wavelength λ_{opt} also becomes significant. However, when the detector plane is tangent to the focal surface at λ_{opt}, in the distribution there appear three maxima (when the VLS grating width exceeds 50 mm); for the design detector position (at 3 mm from the focal surface at the point with λ_{opt}), the intensity is uniformly distributed.

5. Conclusions

We have analysed the capabilities of spherical VLS gratings for use in flat-field spectrographs in the 20–250 Å spectral range. Varying the VLS grating coefficients permits varying the radius of curvature of the wavefront (with coefficient p_1) as well as compensating the aberration of meridional coma (p_2) and spherical aberration (p_3) at a wavelength λ_{opt}. We have analysed the behaviour of spectral focal surfaces of VLS gratings in relation to p_1 and shown the possibility of making VLS spectrographs of two types: flat-field Harada-type spectrographs and spectrographs with a nearly spherical shape of the focal surface (with a constant grating–detector path length), which may be employed for obtaining a high spatial resolution (~10 μm) with a crossed focusing mirror.

Three VLS spectrograph versions of either type were designed (see Table 1); the spectrographs with spatial focusing were calculated for operation in the second diffraction order. In the future, we plan to make a working VLS spectrograph.

Acknowledgements. This work was supported by the Russian Science Foundation (Grant No. 14-12-00506).

References

1. Pirozhkov A.S., Kando M., Esirkepov T.Zh., et al. *Phys. Rev. Lett.*, **108**, 135004 (2012).
2. Kando M., Pirozhkov A.S., Kawase K., et al. *Phys. Rev. Lett.*, **103**, 235003 (2009).
3. Vishnyakov E.A., Shatokhin A.N., Ragozin E.N. *Kvantovaya Elektron.*, **45** (4), 371 (2015) [*Quantum Electron.*, **45** (4), 371 (2015)].
4. *Conf. Program and Book of Abstracts, 15th Intern. Conf. on X-Ray Lasers 2016* (Nara, Japan, 2016) p. 74.
5. Rowland H.A. *Phil. Mag. Ser.* 5, **13** (84), 469 (1882).
6. Samson J.A.R. *Techniques of Vacuum Ultraviolet Spectroscopy* (New York: Wiley, 1967).
7. Harada T., Kita T. *Appl. Opt.*, **19** (23), 3987 (1980).
8. Kita T., Harada T., Nakano N., Kuroda H. *Appl. Opt.*, **22** (4), 512 (1983).
9. Kita T., Harada T. *Appl. Opt.*, **31** (10), 1399 (1992).
10. Harada T., Sakuma H., Takahashi K., Watanabe T., Hara H., Kita T. *Appl. Opt.*, **37** (28), 6803 (1998).
11. Harada T., Moriyama S., Kita T. *Jpn. J. Appl. Phys.*, **14**, Suppl. 14-1, 175 (1975).
12. Gerasimov F.M., Yakovlev E.A., Peisakhson I.V., Koshelev B.V. *Opt. Spektrosk.*, **28** (4), 790 (1970).
13. Dunn J., Magee E.W., Shepherd R., et al. *Rev. Sci. Instrum.*, **79**, 10E314 (2008).
14. Hettrick M.C., Bowyer S., Malina R.F., Martin C., Mrowka S. *Appl. Opt.*, **24** (12), 1737 (1985).
15. Hettrick M.C., Underwood J.H., Batson P.J., Eckart M.J. *Appl. Opt.*, **27** (2), 200 (1988).
16. Hettrick M.C. *Photonics*, **3** (1), 3 (2016).

17. Namioka T. *J. Opt. Soc. Am.*, **49** (5), 446 (1959).
18. http://www.esrf.eu/Instrumentation/software/data-analysis/xop2.3.
19. Kolachevskii N.N., Pirozhkov A.S., Ragozin E.N. *Kvantovaya Elektron.*, **30** (5), 428 (2000) [*Quantum Electron.*, **30** (5), 428 (2000)].
20. Vishnyakov E.A., Kamenets F.F., Kondratenko V.V., et al. *Kvantovaya Elektron.*, **42** (2), 143 (2012) [*Quantum Electron.*, **42** (2), 143 (2012)].
21. Vishnyakov E.A., Mednikov K.N., Pertsov A.A., et al. *Kvantovaya Elektron.*, **39** (5), 474 (2009) [*Quantum Electron.*, **39** (5), 474 (2009)].
22. Ragozin E.N., Mednikov K.N., Pertsov A.A., et al. *Proc. SPIE Int. Soc. Opt. Eng.*, **7360**, 73600N-1-12 (2009).
23. Vishnyakov E.A., Voronov D.L., Gullikson E.M., et al. *Kvantovaya Elektron.*, **43** (7), 666 (2013) [*Quantum Electron.*, **43** (7), 666 (2013)].
24. Zaidel' A.N., Shreider E.Ya. *Vakuumnaya spektroskopiya i ee primenenie* (Vacuum Spectroscopy and its Application) (Moscow: Nauka, 1976).